

OPEN ACCESS

## Repository of the Max Delbrück Center for Molecular Medicine (MDC) in the Helmholtz Association

<http://edoc.mdc-berlin.de/15778>

### Hyper-activation of ATM upon DNA-PKcs inhibition modulates p53 dynamics and cell fate in response to DNA damage

---

Finzel, A., Grybowski, A., Strasen, J., Cristiano, E., Loewer, A.

This is a copy of the final article, which was first published online on June 8, 2016 and in final edited form in:

Molecular Biology of the Cell  
2016 AUG 01; 27(15): 2360-2367  
doi: [10.1091/mbc.E16-01-0032](https://doi.org/10.1091/mbc.E16-01-0032)  
Publisher: [The American Society for Cell Biology \(ASCB\)](http://www.ascb.org)

This article was originally distributed by The American Society for Cell Biology under license from the author(s) and made available to the public two months after publication under the following license:



Copyright © 2016, Finzel et al. This work is licensed under a Creative Commons Attribution-NonCommercial-ShareAlike 3.0 Unported license, as described at <http://creativecommons.org/licenses/by-nc-sa/3.0/>. To view a copy of this license, visit <http://creativecommons.org/licenses/by-nc-sa/3.0/> or send a letter to Creative Commons, PO Box 1866, Mountain View, CA 94042, USA.

# Hyperactivation of ATM upon DNA-PKcs inhibition modulates p53 dynamics and cell fate in response to DNA damage

Ana Finzel<sup>a</sup>, Andrea Grybowski<sup>a</sup>, Jette Strasen<sup>a</sup>, Elena Cristiano<sup>a</sup>, and Alexander Loewer<sup>a,b,\*</sup>

<sup>a</sup>Berlin Institute for Medical Systems Biology, Max Delbrück Center for Molecular Medicine, 13125 Berlin, Germany;

<sup>b</sup>Department of Biology, Technische Universität Darmstadt, 64287 Darmstadt, Germany

**ABSTRACT** A functional DNA damage response is essential for maintaining genome integrity in the presence of DNA double-strand breaks. It is mainly coordinated by the kinases ATM, ATR, and DNA-PKcs, which control the repair of broken DNA strands and relay the damage signal to the tumor suppressor p53 to induce cell cycle arrest, apoptosis, or senescence. Although many functions of the individual kinases have been identified, it remains unclear how they act in concert to ensure faithful processing of the damage signal. Using specific inhibitors and quantitative analysis at the single-cell level, we systematically characterize the contribution of each kinase for regulating p53 activity. Our results reveal a new regulatory interplay in which loss of DNA-PKcs function leads to hyperactivation of ATM and amplification of the p53 response, sensitizing cells for damage-induced senescence. This interplay determines the outcome of treatment regimens combining irradiation with DNA-PKcs inhibitors in a p53-dependent manner.

## Monitoring Editor

Kunxin Luo  
University of California,  
Berkeley

Received: Jan 19, 2016

Revised: May 31, 2016

Accepted: May 31, 2016

## INTRODUCTION

The DNA damage response (DDR) is an essential process that protects the integrity of the genome and prevents cancerogenic transformations. In mammalian cells, sophisticated mechanisms evolved to sense various kinds of DNA damage and adjust cellular physiology by arresting the cell cycle, activating repair mechanisms, or inducing senescence and apoptosis (Ciccia and Elledge, 2010). Among the most dangerous DNA lesions are double-strand breaks (DSBs), as they can lead to chromosomal aberrations and cellular transformation when left unrepaired. Three kinases belonging to the phosphatidylinositol 3-kinase (PI3K)-like kinase family coordinate

the response to DSBs: ataxia telangiectasia-mutated (ATM; Harper and Elledge, 2007), ataxia telangiectasia and Rad3-related (ATR; Cimprich and Cortez, 2008), and DNA-dependent protein kinase catalytic subunit (DNA-PKcs; Chiruvella *et al.*, 2013). The activation of these nuclear serine/threonine kinases follows a complex pattern that changes over time and depends on the cell cycle state, the nature of the induced breaks, and the repair pathways used (Ciccia and Elledge, 2010). ATM is activated immediately upon damage and mediates repair of DSBs by both nonhomologous end joining (NHEJ) and homologous recombination (HR). DNA-PKcs activation, in contrast, is restricted to breaks repaired by canonical NHEJ (cNHEJ). ATR is activated at later stages of the response by the presence of single-stranded DNA, which is mainly exposed during HR.

The activity of the kinases leads to the modification of chromatin and the assembly of large multiprotein complexes around break sites. These irradiation-induced foci serve as platforms to distribute the damage signal throughout the nucleus and activate appropriate repair mechanisms. In addition to organizing repair of DSBs, PI3K-like kinases relay damage signals to p53, the major tumor suppressor in mammalian cells (Lees-Miller *et al.*, 1990). Under nonstressed conditions, p53 is kept at low levels by Mdm2-mediated proteasomal degradation (Figure 1A; Haupt *et al.*, 1997; Kubbutat *et al.*, 1997). When a cell encounters DNA damage, ATM, ATR, and DNA-PK phosphorylate p53 and Mdm2. In addition, ATR and ATM activate the checkpoint kinases Chk1 and Chk2, respectively, which

This article was published online ahead of print in MBoC in Press (<http://www.molbiolcell.org/cgi/doi/10.1091/mbc.E16-01-0032>) on June 8, 2016.

A.F. and A.G. performed the experiments; E.C. and J.S. contributed important reagents; A.F. and A.L. analyzed the data, prepared the figures, and wrote the manuscript; A.L. conceived the study and supervised the research.

\*Address correspondence to: Alexander Loewer ([loewer@bio.tu-darmstadt.de](mailto:loewer@bio.tu-darmstadt.de)).

Abbreviations used: ATM, ataxia telangiectasia-mutated; ATR, ataxia telangiectasia and Rad3-related; DDR, DNA damage response; DNA-PKcs, DNA-dependent protein kinase catalytic subunit; HR, homologous recombination; NHEJ, nonhomologous end joining; PI3K, phosphatidylinositol 3-kinase.

© 2016 Finzel *et al.* This article is distributed by The American Society for Cell Biology under license from the author(s). Two months after publication it is available to the public under an Attribution–Noncommercial–Share Alike 3.0 Unported Creative Commons License (<http://creativecommons.org/licenses/by-nc-sa/3.0>).

“ASCB,” “The American Society for Cell Biology®,” and “Molecular Biology of the Cell®” are registered trademarks of The American Society for Cell Biology.

Supplemental Material can be found at:  
<http://www.molbiolcell.org/content/suppl/2016/06/06/mbc.E16-01-0032v1.DC1>

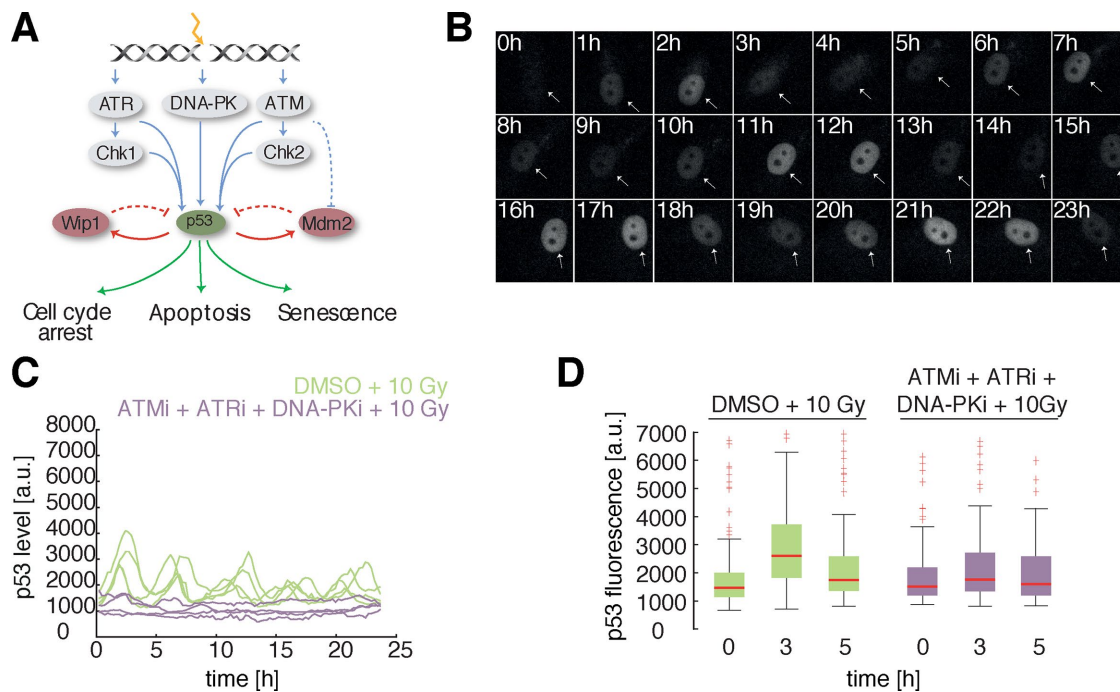


**FIGURE 1:** ATM, ATR, and DNA-PK control the p53 response to DSBs. (A) Schematic overview of the p53 network in response to DSBs. (B) Time-lapse microscopy images of A549 cells expressing p53-YFP after treatment with 10-Gy  $\gamma$ -IR. (C) Individual A549 cells were tracked, and the p53 average nuclear fluorescence intensity was measured in cells untreated or treated with a mix of ATMi, ATRi, and DNA-PKi. (D) Quantification of the p53 average nuclear fluorescence intensity at 0, 3, and 5 h upon 10-Gy  $\gamma$ -IR in A549 cells untreated or treated with a mix of ATMi, ATRi, and DNA-PKi. Red lines indicate medians of distributions; boxes include data between the 25th and 75th percentiles; whiskers extend to maximum values within 1.5 $\times$  the interquartile range; crosses represent outliers (>120 cells/condition).

modify p53 as well (Kruse and Gu, 2009). Together these phosphorylations prevent binding of p53 to Mdm2, which is instead degraded after autoubiquitination. p53 accumulates in the nucleus and acts as a transcription factor promoting the expression of genes involved in DNA repair, cell cycle arrest, apoptosis, and senescence in order to maintain genome integrity (Vousden and Prives, 2009). Among these p53 target genes is the negative regulator Mdm2, whose expression terminates the p53 response through a negative feedback loop. A second feedback loop exists between p53 and Wip1, a phosphatase that reverses phosphorylation by PI3K-like kinases (Lu *et al.*, 2007; Batchelor *et al.*, 2008). These two interlinked negative feedback loops shape the dynamic response of p53 to DSBs, resulting in pulsatile protein accumulations with uniform amplitudes and durations, independent of the degree of damage (Lahav *et al.*, 2004). When the properties of these p53 pulses were perturbed, either genetically or pharmacologically, the cellular response to damage was changed, highlighting the importance of p53 dynamics for regulating cell fate decisions (Purvis *et al.*, 2012; Borcherds *et al.*, 2014).

Medically, induction of DNA damage is used as cancer treatment during chemotherapy and radiotherapy. A promising strategy to further increase the efficiency of such treatments is to sensitize cancer cells by targeted perturbations of DDR pathways. Initial studies using *in vitro* models, xenografts, or first clinical trials demonstrated the feasibility of this approach for ATM, ATR, or DNA-PKcs inhibitors (Davidson *et al.*, 2013; Weber and Ryan, 2015). However, to gain a deeper understanding of the molecular mechanisms underlying the sensitizing effect of these inhibitors, it is important to understand how the individual kinases interact with each other and with cell regulatory networks such as the p53 pathway. Owing to the complex

pattern of kinase activation, each kinase may play a distinct role in controlling the dynamic response of p53. Alternatively, they may be able to compensate each other's function in relaying the damage signal to preserve genomic integrity. Moreover, it is at present unclear to what extent these kinases function independently from each other or modulate each other's activity in regard to p53 activation. Finally, we need to understand how the sensitizing effect of kinase inhibitors depends on the state of the targeted cell—for example, p53 mutations present in a given tumor.

To systematically address these questions, we used fluorescent reporters, live-cell time-lapse microscopy, and automated image analysis in combination with pharmacological perturbations to follow the p53 response upon induction of DSBs with ionizing  $\gamma$ -irradiation (IR) in individual cells with high temporal and spatial resolution. Using this approach, we found a new regulatory loop between DNA-PKcs, ATM, and p53 that contributes to sensitizing cells to radiation by increased induction of senescence.

## RESULTS AND DISCUSSION

### Inhibition of DNA-PKcs induces an amplified p53 response

To follow the p53 response over time, we used clonal cell lines stably expressing p53 fused to the yellow fluorescent protein Venus (p53-YFP; Supplemental Figure S1A). These included the transformed cell lines A549, U-2 OS, and MCF7 (Batchelor *et al.*, 2008; Chen *et al.*, 2013), as well as the untransformed cell line MCF10A (this study). As previously reported, p53-YFP protein accumulated in regular pulses upon damage induction (Figure 1, B and C). To characterize p53 dynamics, we analyzed hundreds of single-cell trajectories and extracted features such as pulse width and amplitude (Supplemental Figure S1, B and C). Because p53 pulses are uniform over

time, we report only the properties of the first response here. Our results confirmed that in A549 and MCF10A cells, features of the first p53 pulse are constant across increasing doses of  $\gamma$ -IR and therefore independent of the number of DSBs induced (Supplemental Figure S1, D and E; Lahav *et al.*, 2004).

To systematically study the role of all three PI3K-like kinases in shaping the p53 response, we used well-characterized small-molecule inhibitors (KU-55933, ATM inhibitor [ATMi]; VE-821, ATR inhibitor [ATRi]; and NU 7026, DNA-PK inhibitor [DNA-PKi]) and confirmed their specificity using Western blot analysis (Supplemental Figure S1F; Hickson *et al.*, 2004; Reaper *et al.*, 2011). When we applied all three inhibitors together before treating cells with  $\gamma$ -IR, we no longer observed a p53 response in both A549 and MCF10A cells, as expected (Figure 1, C and D, and Supplemental Figure S1G). Next we investigated whether these kinases act as redundant systems to provide a fail-safe relay of the damage input to the p53 system or whether each of them performs a distinct function. We first inhibited ATM, which has been described as the main kinase inducing p53 accumulation upon DSB induction (Ciccia and Elledge, 2010). However, we did not observe qualitative differences in p53 pulses (Figure 2A). When we quantified the first p53 pulse, we detected only a slight reduction of pulse amplitude, whereas pulse duration remained unaltered (Figure 2B and Supplemental Figure S2, A, B, and D). This indicated that under the given experimental conditions, loss of ATM activity was compensated by the other PI3K-like kinases, which is consistent with previous studies in ATM-deficient cells (Li and Stern, 2005; Boehme *et al.*, 2008; Callén *et al.*, 2009; Tomimatsu *et al.*, 2009). Next we inhibited ATR. Again, we observed regular p53 pulses with only a small decrease in amplitude (Figure 2, A and B, and Supplemental Figure S2, A, B, and D). This compensation of ATR activity is in line with its secondary role during the DSB response, in which its function in the presence of ATM is restricted to contributing to damage repair by HR (Cimprich and Cortez, 2008).

When we finally inhibited DNA-PKcs, we unexpectedly observed a strong alteration of p53 dynamics upon  $\gamma$ -IR: the first response was longer and of increased amplitude across different transformed and untransformed cell lines (Figure 2, A and B, and Supplemental Figure S2, A–G). To validate these results, we used an alternative DNA-PKcs inhibitor (NU 7441, DNA-PKi-2) and observed a similarly amplified response (Figure 2B and Supplemental Figure S2, A, B, and D). Moreover, we analyzed endogenous p53 by Western blot and confirmed higher p53 protein levels and a longer duration of the first response (Supplemental Figure S2H). Of interest, this increase in p53 levels was not noticed in previous studies (Zhu and Gooderham, 2006; Shaheen *et al.*, 2011). Because these used measurements at constrained number of time points, the amplification of the p53 response might have been not as obvious as in the time-resolved, single-cell measurements presented here.

### Loss of DNA-PK activity modulates the p53 response through prolonged activation of ATM

How does inhibition of a kinase involved in relaying the damage signal lead to an amplified p53 response? Because DNA-PKcs plays a critical role in cNHEJ and loss of its activity leads to a reduced repair rate (Loewer *et al.*, 2013), we initially hypothesized that the observed changes in p53 dynamics might occur due to an increase in the number of DSBs. We therefore measured p53 dynamics in the presence or absence of DNA-PKi after damaging cells with different irradiation doses. In untreated cells, p53 accumulation was hardly changed, even when we induced four times as

many DSBs (compare 2.5 to 10 Gy). In contrast, when DNA-PKcs was inhibited, the width and amplitude of p53 pulses increased in a dose-dependent manner (Figure 2C and Supplemental Figures S2, C and E–G, and S3, A–C).

To investigate further whether p53 dynamics is in general affected by altered DSBs repair, we used an inhibitor against another component of the cNHEJ pathway, ligase IV (SCR7, LigIVi), which caused a decreased repair rate when applied to cells before genotoxic stress (Supplemental Figure S3D; Srivastava *et al.*, 2012). However, cells treated with this inhibitor did not show changes in p53 dynamics (Figure 2D and Supplemental Figure S3E), suggesting that an increase in unrepaired DSBs alone is not sufficient for amplifying the p53 response.

As an alternative hypothesis, we considered that inhibiting DNA-PKcs altered the interplay between the PI3K-like kinases. We therefore performed pairwise inhibition of all three kinases. When we inhibited both DNA-PKcs and ATR, we again observed longer and stronger accumulation of p53 compared with untreated cells (Figure 3A and Supplemental Figure S3F). However, combining DNA-PKi and ATMi before damage induction surprisingly reverted the phenotype of DNA-PKcs inhibition: when we measured the resulting p53 response in living cells, we found that pulse duration was reduced from ~200 min for cells treated with DNA-PKi alone to ~100 min as in controls (Figure 3B and Supplemental Figure S3G). The amplitude was similarly reduced. Inhibiting both ATM and ATR also resulted in p53 dynamics almost indistinguishable from that of untreated cells, albeit slightly more irregular (Figure 3C and Supplemental Figure S3H). These results indicate that ATR and DNA-PKcs alone induce regular p53 dynamics and are able to compensate the loss of the two other kinases. In contrast, p53 reacts more strongly to DNA damage when ATM is active in the absence of a functional DNA-PKcs kinase, independently of ATR's state.

We hypothesized that this amplified p53 response is caused by hyperactivation of ATM in the presence of DNA-PKi. To test this, we measured ATM autophosphorylation at Ser-1981 and Chk2 phosphorylation at Thr-68 as surrogates for ATM's activation state and observed an increase in their levels after damage in the presence of DNA-PKcs inhibitor (Figure 3D), which was reverted by ATMi treatment. We then analyzed the levels of phosphorylated Chk2 and p53 over time in the presence and absence of DNA-PKi and observed a dramatic increase in the amount and duration of both modifications (Figure 3E). At the same time, protein levels of Mdm2, which is autodegraded in an ATM-dependent manner (Stommel and Wahl, 2004), were severely decreased. We verified that lower Mdm2 levels were due to posttranslational regulation by measuring its mRNA levels as well as mRNA levels of Wip1, another negative regulator of p53. As expected, we only observed minor differences during the first hours after damage (Supplemental Figure S4A). To understand whether ATM influences p53 dynamics through Mdm2, Chk2, or both, we analyzed the p53 response in single cells upon simultaneous inhibition of Chk2 and DNA-PKcs. Because we still observed an amplified p53 response under this condition (Supplemental Figure S4, B and C), we concluded that increased Chk2 activity is a secondary effect and not involved in altering p53 dynamics.

Taking the results together, we were able to show for the first time that inhibiting DNA-PKcs leads to a dose-dependent hyperactivation of ATM upon DSBs induction, which induces Mdm2 degradation and increased accumulation of p53. This new interplay between the two PI3K-like kinases could be mediated by direct modification of ATM or indirectly by a failure of DNA-PKcs to perform its function at the break site. It is well established that ATM can

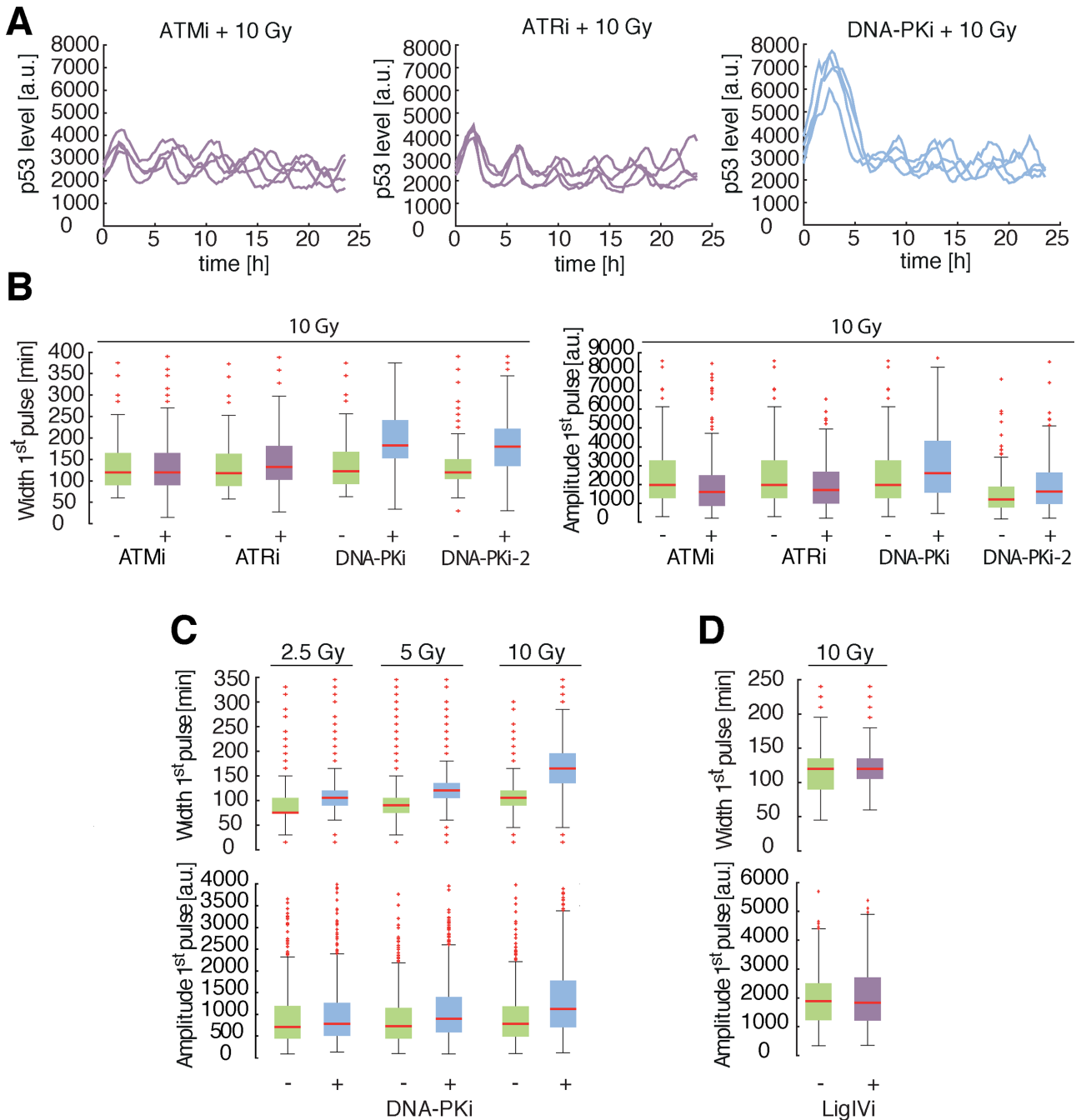


**FIGURE 2:** DNA-PKcs inhibition induces an amplified p53 response. (A) Individual A549 cells were tracked, and the average nuclear fluorescence was measured upon 10-Gy  $\gamma$ -IR in cells treated with ATMi, ATRi, or DNA-PKi as indicated. (B–D) Quantification of the relative amplitude and full-width at half-maximum (FWHM) of the first p53 pulse in A549 cells upon (B) 10-Gy  $\gamma$ -IR in cells untreated or treated individually with ATMi, ATRi, DNA-PKi, or DNA-PKi-2 (>130 cells/condition), (C) 2.5, 5, or 10 Gy in cells untreated or treated with DNA-PKi (>730 cells/condition), or (D) 10-Gy  $\gamma$ -IR untreated or treated with LigIV inhibitor (>170 cells/condition). For statistical analysis, see Supplemental Figures S2 and S3.

phosphorylate DNA-PK at two defined S/TQ clusters and thereby regulate its activity within the cNHEJ pathway (Chen *et al.*, 2007). It is conceivable that DNA-PKcs in turn phosphorylates ATM and inhibits it. Alternatively, it was previously shown that inactive DNA-PKcs inhibits processing of DSBs, keeping them in an immature state (Jiang *et al.*, 2015), which may continuously signal to and activate ATM. Of interest, a recent study reported ATM hyperactivation upon oxidative stress in DNA-PKcs-deficient cells, albeit indepen-

dent of DNA-PKcs function in NHEJ (Li *et al.*, 2014). In any case, hyperactivation of ATM could serve as an important fail-safe mechanism for insults that cannot be easily repaired, such as complex break sites consisting of multiple DSBs in close vicinity. In this case, hyperactivation of ATM might alter the repair pathway choice by forcing end resection (Zhou and Paull, 2013) and ensure that the presence of the severe damage is transmitted to response pathways such as p53.

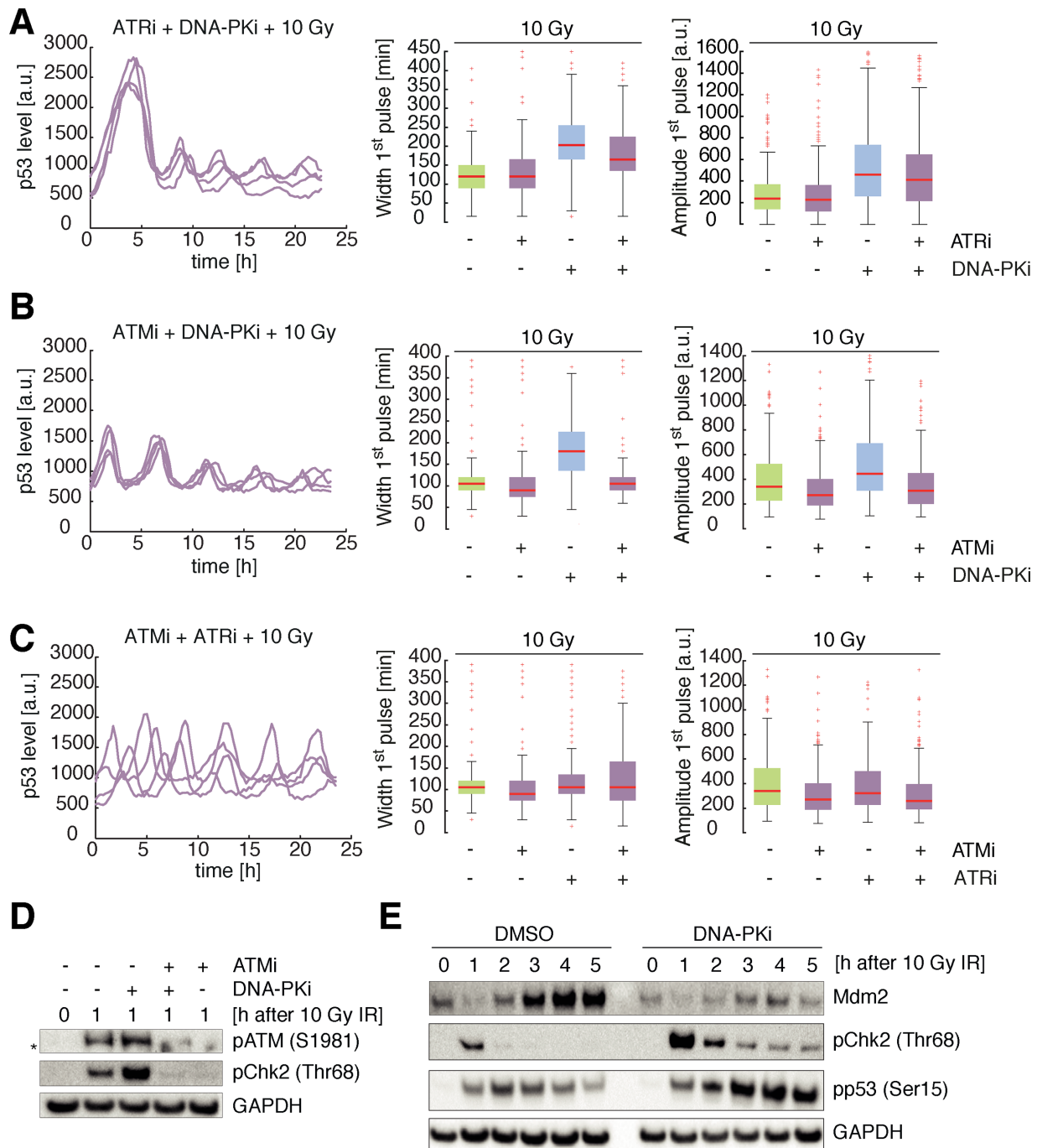


**FIGURE 3:** Loss of DNA-PKcs activity modulates the p53 response through hyperactivation of ATM. (A–C) Individual trajectories and quantification of the relative amplitude and FWHM of the first p53 pulse upon 10-Gy  $\gamma$ -IR in A549 cells untreated or treated with (A) DNA-PKi and ATRi (>280 cells/condition), (B) DNA-PKi and ATMi (>260 cells/condition), or (C) ATMi and ATRi (>260 cells/condition) alone or in combination. (D) Analysis of ATM activity (measured by Western blotting with pATM- and pChk2-specific antibodies) in A549 cells untreated or treated with DNA-PKi and ATMi alone or a combination of both, followed by 10-Gy  $\gamma$ -IR. Asterisk indicates a nonspecific band. (E) Western blot analysis of Mdm2, pChk2, pp53, and GAPDH upon 10-Gy  $\gamma$ -IR in A549 cells untreated or treated with DNA-PKi. For statistical analysis, see Supplemental Figure S3.

### Modulation of p53 dynamics leads to altered cell fate decision upon DSB induction

Previous studies showed that changes in p53 dynamics lead to altered expression of target genes and cell fate decisions (Purvis *et al.*, 2012; Borchers *et al.*, 2014). To address whether altered

p53 accumulation upon DNA-PKcs inhibition modulates how cells react to DSBs, we first tested the induction of the p53 target genes p21, involved in cell cycle arrest, and YPEL3, involved in senescence. We observed strongly increased induction of both target genes in the absence of DNA-PKcs activity 1 and 2 d after

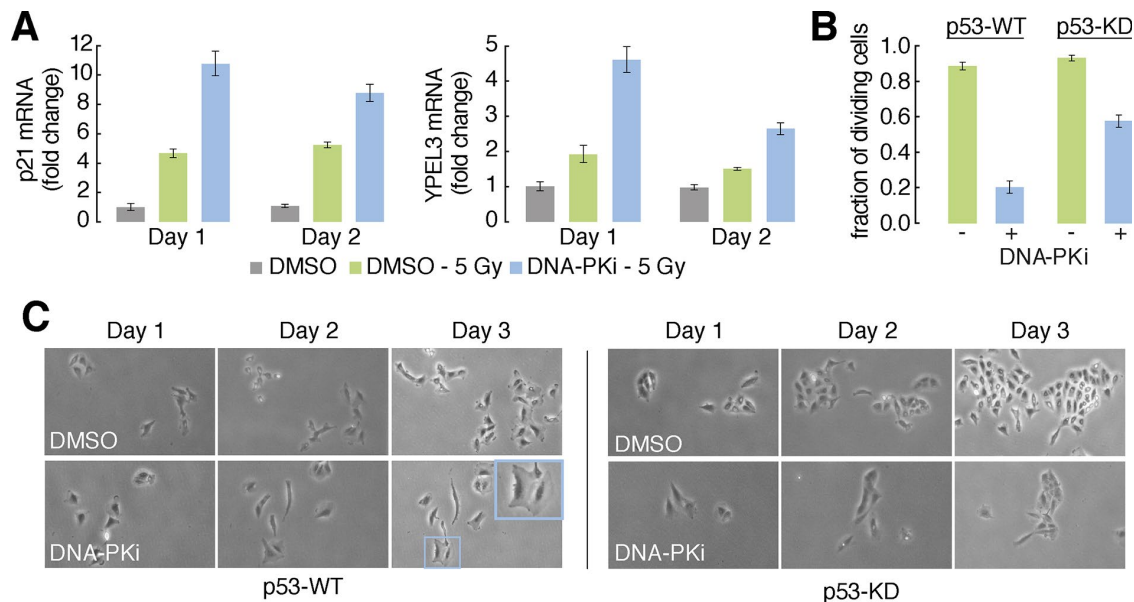


**FIGURE 4:** Prolonged p53 activation leads to altered cell fate decision upon DSB induction. (A) mRNA expression of p53 target genes p21 and YPEL3 was measured at days 1 and 2 in unirradiated A549 cells or upon 5-Gy  $\gamma$ -IR in cells untreated or treated with DNA-PKi.  $\beta$ -Actin was used as an internal control. Error bars indicate SD of technical triplicates. (B) Percentage of dividing A549 cells during 3 d after damage (5-Gy  $\gamma$ -IR) in wild-type (WT) or p53-knockdown (KD) conditions in the presence or absence of DNA-PKi. Error bars indicate SE of sample proportion. Initial number of cells, >125/condition. (C) Representative images of single A549 cells during 3 d upon 5-Gy  $\gamma$ -IR in cells untreated or treated with DNA-PKi in WT or p53 KD conditions. Blue boxes highlight the senescence-like phenotype observed in p53 WT cells treated with DNA-PKi.

irradiation (Figure 4A). Is this sufficient to change the fate of damaged cells? We followed control and DNA-PKi-treated cells for 3 d after irradiation with 5-Gy  $\gamma$ -IR and observed a dramatic decrease in proliferation in treated cells (Figure 4, B and C). In addition, they acquired a flattened morphology characteristic of senescence and expressed senescence-associated  $\beta$ -galactosidase (Supplemental Figure S4D). The decrease in cell proliferation was mostly driven by p53, as the majority of cells lacking the tumor suppressor due to small interfering RNA-mediated knockdown were able to proliferate even in the presence of the inhibitor. Whereas combined treatment with DNA-PKCs and ATM inhibitors was sufficient to revert the amplified p53 response to acute damage, it led to a p53-independent increase in senescence cells due to secondary effects during DNA repair.

It is well established that DNA-PKCs inhibition sensitizes cells for radiation (Davidson *et al.*, 2013). However, this has been mainly attributed to its function in cNHEJ. Only few studies reported that the radiosensitizing effect depends on the genotype—for example, the p53 status (Shaheen *et al.*, 2011). Our results indicate that the observed radiosensitivity is at least in part caused by hyperactivation of ATM that causes an altered p53 response. This has implications for the use of DNA-PK inhibitors in cancer therapies. Although tumors that retain a wild-type copy of p53 might respond well to a combination of radiotherapy and DNA-PKi, cells with mutated p53 might be less affected. On the contrary, neighboring healthy cells with intact p53 might be more severely affected in this scenario, increasing the side effects of tumor therapy. It will therefore be important to characterize the individual state of a given tumor to devise an efficient strategy to specifically kill transformed cells while ensuring survival of neighboring tissues.

## MATERIALS AND METHODS

### Cells

We maintained all A549 and U-2 OS cell lines in McCoy's 5A (GE Healthcare Life Sciences, Freiburg, Germany) plus 10% fetal calf serum (FCS; Thermo Fisher Scientific, Darmstadt, Germany); all MCF10A cell lines in DMEM/F-12 (Thermo Fisher Scientific) plus 5% horse serum (PAN-Biotech, Aidenbach, Germany), 20 ng/ml epidermal growth factor (EGF; Peptrotech, Hamburg, Germany), 0.5  $\mu$ g/ml hydrocortisone (Sigma-Aldrich, München, Germany), 100 ng/ml cholera toxin (Sigma-Aldrich), and 10  $\mu$ g/ml insulin (Sigma-Aldrich); and MCF7 cells in RPMI 1640 (Thermo Fisher Scientific) plus 10% FCS at 37°C. All media contained penicillin and streptomycin. When appropriate, selective antibiotics (400  $\mu$ g/ml G418 (Carl Roth, Karlsruhe, Germany), 50  $\mu$ g/ml hygromycin (Thermo Fisher Scientific), or 0.5  $\mu$ g/ml puromycin [Carl Roth]) were added to maintain transgene expression.

The A549, U-2 OS (Chen *et al.*, 2013), and MCF7 (Batchelor *et al.*, 2008) p53-Venus reporter cell lines have been described before. We generated p53 fluorescent reporters in MCF10A by infecting cells with lentiviruses encoding a construct in which p53 was fused to Venus fluorescent protein under the control of the human ubiquitin C promoter (UbCp).

We added nuclear markers to reporters by infecting with lentiviruses expressing histone 2B fused to cyan fluorescent protein (CFP) under the control of UbCp (A549, U-2 OS, and MCF10A) or a near-infrared fluorescent protein (iRFP) with a nuclear localization sequence under the control of the elongation factor 1- $\alpha$  promoter (MCF7). Subsequently, stable clonal cell lines were established and validated. A549 cells expressing p53 shRNA were produced by lentiviral infection and selection with puromycin (Brummelkamp *et al.*, 2002).

For inhibitor treatments, we replaced the medium with a fresh one containing dimethyl sulfoxide (DMSO; Sigma-Aldrich; control), 10  $\mu\text{M}$  KU-55933 (ATMi; Axon Medchem, Groningen, Netherlands), 2  $\mu\text{M}$  VE-821 (ATRi; Selleckchem, München, Germany), 10  $\mu\text{M}$  NU7026 (DNA-PKi; Biomol, Hamburg, Germany), 1  $\mu\text{M}$  NU7441 (DNA-PKi-2, DNA-PKcs inhibitor; Axon Medchem), 10  $\mu\text{M}$  Chk2 inhibitor II (Chk2i II; Millipore, Darmstadt, Germany), and 100  $\mu\text{M}$  SCR7 (LigIV, ligase IV inhibitor; Xcess Biosciences, San Diego, CA) alone or in combination 30 min before irradiating cells using a cesium-137  $\gamma$ -ray source.

### Western blot analysis

We harvested cells, lysed them in the presence of protease and phosphatase inhibitors, and extracted proteins, which we quantified using bicinchoninic acid assay. Equal protein amounts were separated by electrophoreses on 4–12% Bis-Tris or 3–8% Tris-acetate gradient gels (Thermo Fisher Scientific) and transferred to nitrocellulose or polyvinylidene fluoride membranes (Carl Roth), respectively, by electroblotting (overnight for Tris-acetate gels). We blocked membranes with 5% nonfat dried milk (Carl Roth) or 5% bovine serum albumin (Carl Roth) and incubated them overnight with primary antibody. The next day, we washed the membranes, incubated them with secondary antibody coupled to peroxidase, and washed them again. Protein levels were detected using chemiluminescence (ECL Prime, Amersham).

We used antibodies against total p53 (FL-393), Mdm2 (SMP14), and total DNA-PKcs (H163) from Santa Cruz Biotechnology (Dallas, TX); phospho-Chk1 (Ser-317), phospho-Chk2 (Thr-68), and phospho-p53 (Ser-15) from Cell Signaling (Danvers, MA); phospho-ATM (S1981) from Rockland (Limerick, PA); phospho-histone H2A.X (Ser-319, JBW301) from Millipore; phospho-DNA-PKcs (S2056) from Abcam (Cambridge, MA); and glyceraldehyde-3-phosphate dehydrogenase from Sigma-Aldrich.

### Time-lapse microscopy

We seeded cells in poly-D-lysine-coated glass-bottom plates (MatTek, Ashland, MA) 2 d before experiments. The day of the experiment, medium was replaced with a fresh one without phenol red and riboflavin. We imaged cells on a Nikon Ti inverted fluorescence microscope (Nikon, Düsseldorf, Germany) with a Hamamatsu Orca R2 camera (Hamamatsu, Hamamatsu City, Japan) and a 20 $\times$  Plan Apo objective (numerical aperture [NA] 0.75) using appropriate filter sets (Venus: 500/20-nm excitation [EX], 515-nm dichroic beam splitter [BS], 535/30-nm emission [EM]; CFP: 436/20-nm EX, 455-nm BS, 480/40-nm EX; iRFP: 650/45-nm EX, 685-nm BS, 720/60-nm EX [Chroma]). The microscope was enclosed with an incubation chamber to maintain constant temperature (37°C), CO<sub>2</sub> concentration (5%), and humidity. Cells were imaged every 15 min for the duration of the experiment using Nikon Elements software.

### Image and data analysis

Cells were tracked throughout the duration of the experiment using custom-written Matlab (MathWorks, Natick, MA) scripts based on code developed by the Alon lab (Cohen *et al.*, 2008) and the CellProfiler project (Carpenter *et al.*, 2006). In brief, we applied flat-field correction and background subtraction to raw images before segmenting individual nuclei from nuclear marker images using adaptive thresholding and seeded watershed algorithms. Segmented cells were then assigned to corresponding cells in following images using a greedy match algorithm. Finally, we quantified the nuclear fluorescence intensity of p53-Venus for each cell over time and analyzed the resulting single-cell trajectories computationally to extract

features of p53 dynamics such as amplitude or duration of protein accumulation pulses (Loewer *et al.*, 2010). To determine the effect size and its significance for a given treatment, we calculated changes of the median pulse width and amplitude and performed permutation testing (1000 permutations) to establish corresponding 90% confidence intervals.

### Reverse transcriptase quantitative PCR

We extracted mRNA using High Pure RNA Isolation kits (Roche, Mannheim, Germany). cDNA was generated using M-MuLV reverse transcriptase (NEB, Ipswich, MA) and oligo-dT primers. Quantitative PCR was performed in triplicate using SYBR Green reagent (Roche) on a StepOnePlus PCR machine (Thermo Fisher Scientific). Primer sequences were as follows:  $\beta$ -actin forward, GGC ACC CAG CAC AAT GAA GAT CAA;  $\beta$ -actin reverse, TAG AAG CAT TTG CGG TGG ACG ATG; Wip1 forward, ATA AGC CAG AAC TTC CCA AGG; Wip1 reverse, TGG TCA ATA ACT GTG CTC CTT C; Mdm2 forward, AGA TGT TGG GCC CTT CGT GAG AA; Mdm2 reverse, GCC CTC TTC AGC TTG TGT TGA GTT; p21 forward, TGG ACC TGT CAC TGT CTT GT; p21 reverse, TCC TGT GGG CGG ATT AG; YPEL3 forward, GTG CCT ACC TCT TCA ACT CAG; and YPEL3 reverse, TGC TCT CAA AGG CCT GTT C.

### Immunofluorescence

Cells were grown on coverslips coated with poly-L-lysine (Sigma-Aldrich). The day of the experiment, they were fixed with 2% paraformaldehyde (Carl Roth) and permeabilized with 0.1% Triton X-100 (Carl Roth) in phosphate-buffered saline. We blocked with 10% goat serum (PAN-Biotech) and incubated with pH2A.X (Ser-319) overnight at 4°C. Cells were washed, incubated with secondary antibody coupled to Alexa Fluor 647 (Thermo Fisher Scientific), and washed again. Finally, they were stained with Hoechst and embedded in Prolong Antifade (Thermo Fisher Scientific). Images were acquired with a 60 $\times$  Plan Apo objective (NA 0.75) using appropriate filter sets. Automated segmentation was performed in Matlab (MathWorks) using algorithms from CellProfiler (Carpenter *et al.*, 2006).

### Cell proliferation assay

Cells were seeded 1.5 d before being treated with DMSO or DNA-PKi and irradiated with 5-Gy  $\gamma$ -IR. Medium was changed every day, and the same randomly chosen cells were imaged at days 1, 2, and 3 after irradiation by using gridded dishes and a Nikon Eclipse inverted microscope (Nikon) with a 4 $\times$  objective. Initial numbers and fraction of dividing cells were manually quantified for each condition.

### $\beta$ -Galactosidase assay

Cells were seeded 2 d before being treated with DMSO or DNA-PKi and irradiated with 5 Gy  $\gamma$ -IR. Medium was changed every day. At day 3 after irradiation, cells were fixed with 2% paraformaldehyde/0.2% glutaraldehyde (Sigma-Aldrich) and incubated in staining solution (150 mM NaCl, 40 mM citric acid, 40 mM NaH<sub>2</sub>PO<sub>4</sub>, 2 mM MgCl<sub>2</sub>, 5 mM K<sub>4</sub>(Fe(II)[CN]<sub>6</sub>), 5 mM K<sub>3</sub>(Fe(III)[CN]<sub>6</sub>), and 1 mg/ml X-gal, all Carl Roth) for ~20 h at 37°C. The fractions of stained cells were manually quantified for each condition using gridded dishes.

### ACKNOWLEDGMENTS

We thank Jue Shi (Hong Kong Baptist University, Hong Kong, China) and Galit Lahav (Harvard Medical School, Boston, MA) for sharing cell lines, Gitta Blendinger and Petra Snyder for technical assistance, Marcel Jentsch for help with statistical analysis, and all members of the Loewer lab for helpful discussions.

## REFERENCES

- Batchelor E, Mock CS, Bhan I, Loewer A, Lahav G (2008). Recurrent initiation: a mechanism for triggering p53 pulses in response to DNA damage. *Mol Cell* 30, 277–289.
- Boehme KA, Kulikov R, Blattner C (2008). p53 stabilization in response to DNA damage requires Akt/PKB and DNA-PK. *Proc Natl Acad Sci USA* 105, 7785–7790.
- Borcherds W, Theillet F-X, Katzer A, Finzel A, Mishall KM, Powell AT, Wu H, Manieri W, Dieterich C, Selenko P, et al. (2014). Disorder and residual helicity alter p53-Mdm2 binding affinity and signaling in cells. *Nat Chem Biol* 10, 1000–1002.
- Brummelkamp TR, Bernards R, Agami R (2002). Stable suppression of tumorigenicity by virus-mediated RNA interference. *Cancer Cell* 2, 243–247.
- Callén E, Jankovic M, Wong N, Zha S, Chen H-T, Difiilippantonio S, Di Virgilio M, Heidkamp G, Alt FW, Nussenzweig A, et al. (2009). Essential role for DNA-PKcs in DNA double-strand break repair and apoptosis in ATM-deficient lymphocytes. *Mol Cell* 34, 285–297.
- Carpenter AE, Jones TR, Lamprecht MR, Clarke C, Kang I, Friman O, Guertin DA, Chang J, Lindquist RA, Moffat J, et al. (2006). CellProfiler: image analysis software for identifying and quantifying cell phenotypes. *Genome Biol* 7, R100.
- Chen X, Chen J, Gan S, Guan H, Zhou Y, Ouyang Q, Shi J (2013). DNA damage strength modulates a bimodal switch of p53 dynamics for cell-fate control. *BMC Biol* 11, 73.
- Chen BPC, Uematsu N, Kobayashi J, Lerenthal Y, Krempler A, Yajima H, Löbrich M, Shiloh Y, Chen DJ (2007). Ataxia telangiectasia mutated (ATM) is essential for DNA-PKcs phosphorylations at the Thr-2609 cluster upon DNA double strand break. *J Biol Chem* 282, 6582–6587.
- Chiruvella KK, Liang Z, Wilson TE (2013). Repair of double-strand breaks by end joining. *Cold Spring Harb Perspect Biol* 5, a012757.
- Ciccia A, Elledge SJ (2010). The DNA damage response: making it safe to play with knives. *Mol Cell* 40, 179–204.
- Cimprich KA, Cortez D (2008). ATR: an essential regulator of genome integrity. *Nat Rev Mol Cell Biol* 9, 616–627.
- Cohen AA, Geva-Zatorsky N, Eden E, Frenkel-Morgenstern M, Issaeva I, Sigal A, Milo R, Cohen-Saidon C, Liron Y, Kam Z, et al. (2008). Dynamic proteomics of individual cancer cells in response to a drug. *Science* 322, 1511–1516.
- Davidson D, Amrein L, Panasci L, Aloyz R (2013). Small molecules, inhibitors of DNA-PK, targeting DNA repair, and beyond. *Front Pharmacol* 4, 5.
- Harper JW, Elledge SJ (2007). The DNA damage response: ten years after. *Mol Cell* 28, 739–745.
- Haupt Y, Maya R, Kazaz A, Oren M (1997). Mdm2 promotes the rapid degradation of p53. *Nature* 387, 296–299.
- Hickson I, Zhao Y, Richardson CJ, Green SJ, Martin NMB, Orr AI, Reaper PM, Jackson SP, Curtin NJ, Smith GCM (2004). Identification and characterization of a novel and specific inhibitor of the ataxia-telangiectasia mutated kinase ATM. *Cancer Res* 64, 9152–9159.
- Jiang W, Crowe JL, Liu X, Nakajima S, Wang Y, Li C, Lee BJ, Dubois RL, Liu C, Yu X, et al. (2015). Differential phosphorylation of DNA-PKcs regulates the interplay between end-processing and end-ligation during nonhomologous end-joining. *Mol Cell* 58, 172–185.
- Kruse J-P, Gu W (2009). Modes of p53 regulation. *Cell* 137, 609–622.
- Kubbutat MHG, Jones SN, Vousden KH (1997). Regulation of p53 stability by Mdm2. *Nature* 387, 299–303.
- Lahav G, Rosenfeld N, Sigal A, Geva-Zatorsky N, Levine AJ, Elowitz MB, Alon U (2004). Dynamics of the p53-Mdm2 feedback loop in individual cells. *Nat Genet* 36, 147–150.
- Lees-Miller SP, Chen YR, Anderson CW (1990). Human cells contain a DNA-activated protein kinase that phosphorylates simian virus 40 T antigen, mouse p53, and the human Ku autoantigen. *Mol Cell Biol* 10, 6472–6481.
- Li J, Stern DF (2005). Regulation of CHK2 by DNA-dependent protein kinase. *J Biol Chem* 280, 12041–12050.
- Li M, Lin Y-F, Palchik GA, Matsunaga S, Wang D, Chen BPC (2014). The catalytic subunit of DNA-dependent protein kinase is required for cellular resistance to oxidative stress independent of DNA double-strand break repair. *Free Radic Biol Med* 76, 278–285.
- Loewer A, Batchelor E, Gaglia G, Lahav G (2010). Basal dynamics of p53 reveal transcriptionally attenuated pulses in cycling cells. *Cell* 142, 89–100.
- Loewer A, Karanam K, Mock C, Lahav G (2013). The p53 response in single cells is linearly correlated to the number of DNA breaks without a distinct threshold. *BMC Biol* 11, 114.
- Lu X, Ma O, Nguyen T-A, Jones SN, Oren M, Donehower LA (2007). The Wip1 phosphatase acts as a gatekeeper in the p53-Mdm2 autoregulatory loop. *Cancer Cell* 12, 342–354.
- Purvis JE, Karhohs KW, Mock C, Batchelor E, Loewer A, Lahav G (2012). p53 dynamics control cell fate. *Science* 336, 1440–1444.
- Reaper PM, Griffiths MR, Long JM, Charrier J-D, MacCormick S, Charlton PA, Golec JMC, Pollard JR (2011). Selective killing of ATM- or p53-deficient cancer cells through inhibition of ATR. *Nat Chem Biol* 7, 428–430.
- Shaheen FS, Znojek P, Fisher A, Webster M, Plummer R, Gaughan L, Smith GCM, Leung HY, Curtin NJ, Robson CN (2011). Targeting the DNA double strand break repair machinery in prostate cancer. *PLoS One* 6, e20311.
- Srivastava M, Nambiar M, Sharma S, Karki SS, Goldsmith G, Hegde M, Kumar S, Pandey M, Singh RK, Ray P, et al. (2012). An inhibitor of nonhomologous end-joining abrogates double-strand break repair and impedes cancer progression. *Cell* 151, 1474–1487.
- Stommel JM, Wahl GM (2004). Accelerated MDM2 auto-degradation induced by DNA-damage kinases is required for p53 activation. *EMBO J* 23, 1547–1556.
- Tomimatsu N, Mukherjee B, Burma S (2009). Distinct roles of ATR and DNA-PKcs in triggering DNA damage responses in ATM-deficient cells. *EMBO Rep* 10, 629–635.
- Vousden KH, Prives C (2009). Blinded by the light: the growing complexity of p53. *Cell* 137, 413–431.
- Weber AM, Ryan AJ (2015). ATM and ATR as therapeutic targets in cancer. *Pharmacol Ther* 149, 124–138.
- Zhou Y, Paull TT (2013). DNA-dependent protein kinase regulates DNA end resection in concert with Mre11-Rad50-Nbs1 (MRN) and ataxia telangiectasia-mutated (ATM). *J Biol Chem* 288, 37112–37125.
- Zhu H, Gooderham NJ (2006). Mechanisms of induction of cell cycle arrest and cell death by cryptolepine in human lung adenocarcinoma a549 cells. *Toxicol Sci* 91, 132–139.

# Supplemental Materials

*Molecular Biology of the Cell*

Finzel et al.

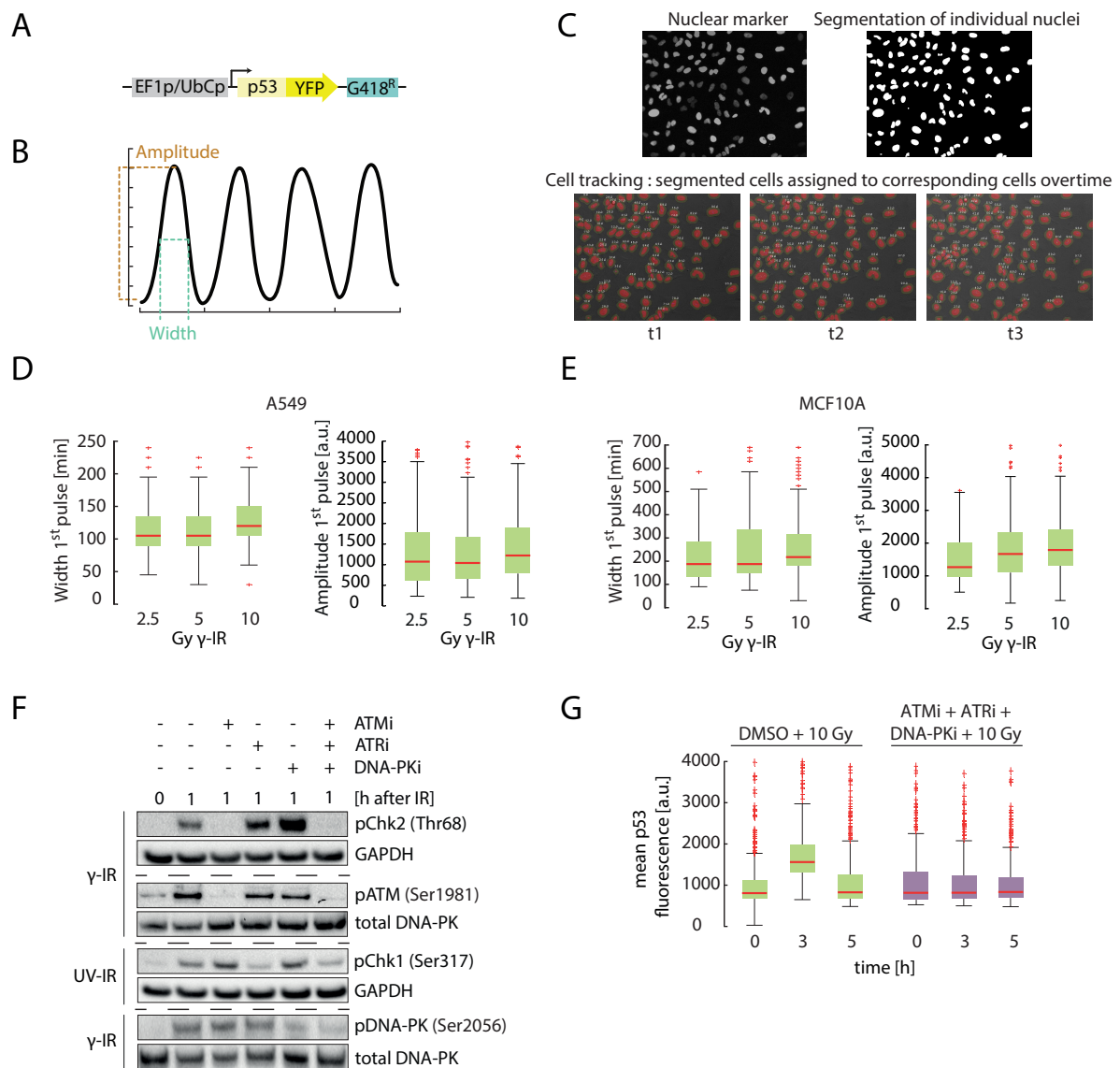


**Figure S1.** (A) Scheme of the p53 fluorescent reporter construct. (B) Schematic drawing of the dynamic features (relative amplitude and full width at half maximum (FWHM)) of the first p53 pulse. (C) Image analysis example: cells are segmented according to the nuclear marker; segmented cells are assigned to corresponding cells at following time-points. See experimental procedures for details. (D-E) Quantification of the relative amplitude and FWHM of the first p53 pulse upon 2.5, 5 or 10 Gy  $\gamma$ -IR for (D) A549 ( $n > 250$  cells per condition) or (E) MCF10A cells ( $n > 42$  cells per condition). (F) Western blot analysis showing specificity of ATMi (measured by pATM and pChk2), of ATRi (measured by pChk1) and DNA-PKi (measured by pDNA-PK) in A549 cells. Cells were treated with 10 Gy  $\gamma$ -IR or 4.5 J/m<sup>2</sup> ultraviolet (UV) radiation. (G) Quantification at 0, 3 and 5 hours of the p53 average nuclear fluorescence intensity upon 10 Gy  $\gamma$ -IR in MCF10A cells untreated or treated with a mix of ATMi, ATRi and DNA-PKi. ( $n > 430$  cells per condition)

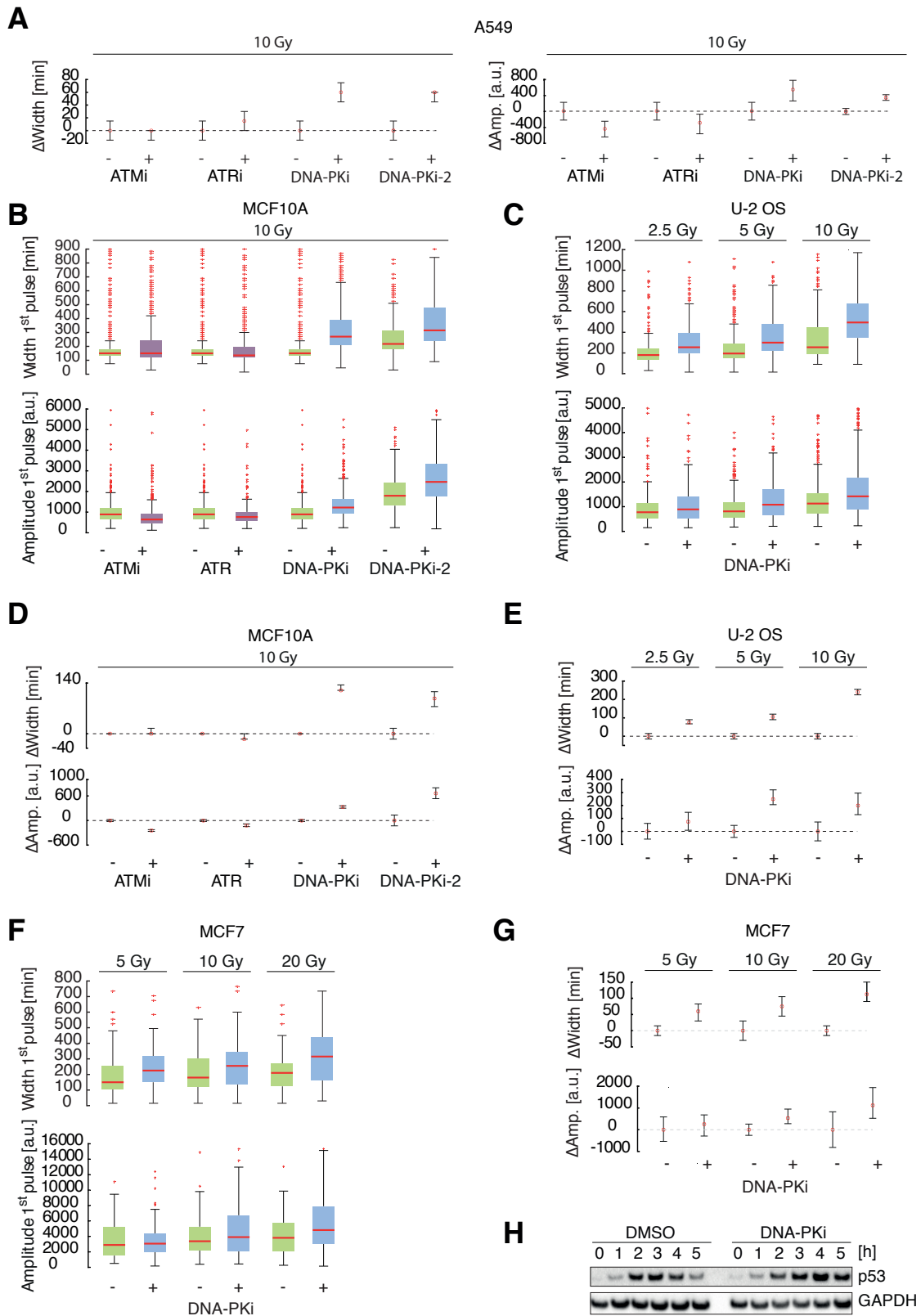


**Figure S2.** (A) Statistical analysis corresponding to Figure 2B. Estimated changes of the median pulse width and amplitude (red dots); error bars represent 90% confidence intervals. (B) Quantification of the relative amplitude and FWHM of the first p3 pulse upon 10 Gy  $\gamma$ -IR in MCF10A cells untreated or treated with ATMi, ATRi, DNA-PKi or DNA-PKi-2. ( $n >$

210 cells per condition). (C) Quantification of the relative amplitude and FWHM of the first p53 pulse upon 2.5, 5 or 10 Gy in cells untreated or treated with DNA-PKi in U-2 OS ( $n > 250$  cells per condition). (D-E) Statistical analysis corresponding to Figure S2B. and S2C. Estimated changes of the median pulse width and amplitude (red dots); error bars represent 90% confidence intervals. (F-G) Quantification of the relative amplitude and FWHM of the first p53 pulse upon 5, 10 or 20 Gy in cells untreated or treated with DNA-PKi in MCF7 and corresponding statistical analysis (error bars represent 90% confidence intervals,  $n > 85$  cells per condition). (H) Western blot analysis of total p53 upon 10 Gy  $\gamma$ -IR in A549 cells untreated or treated with DNA-PKi.

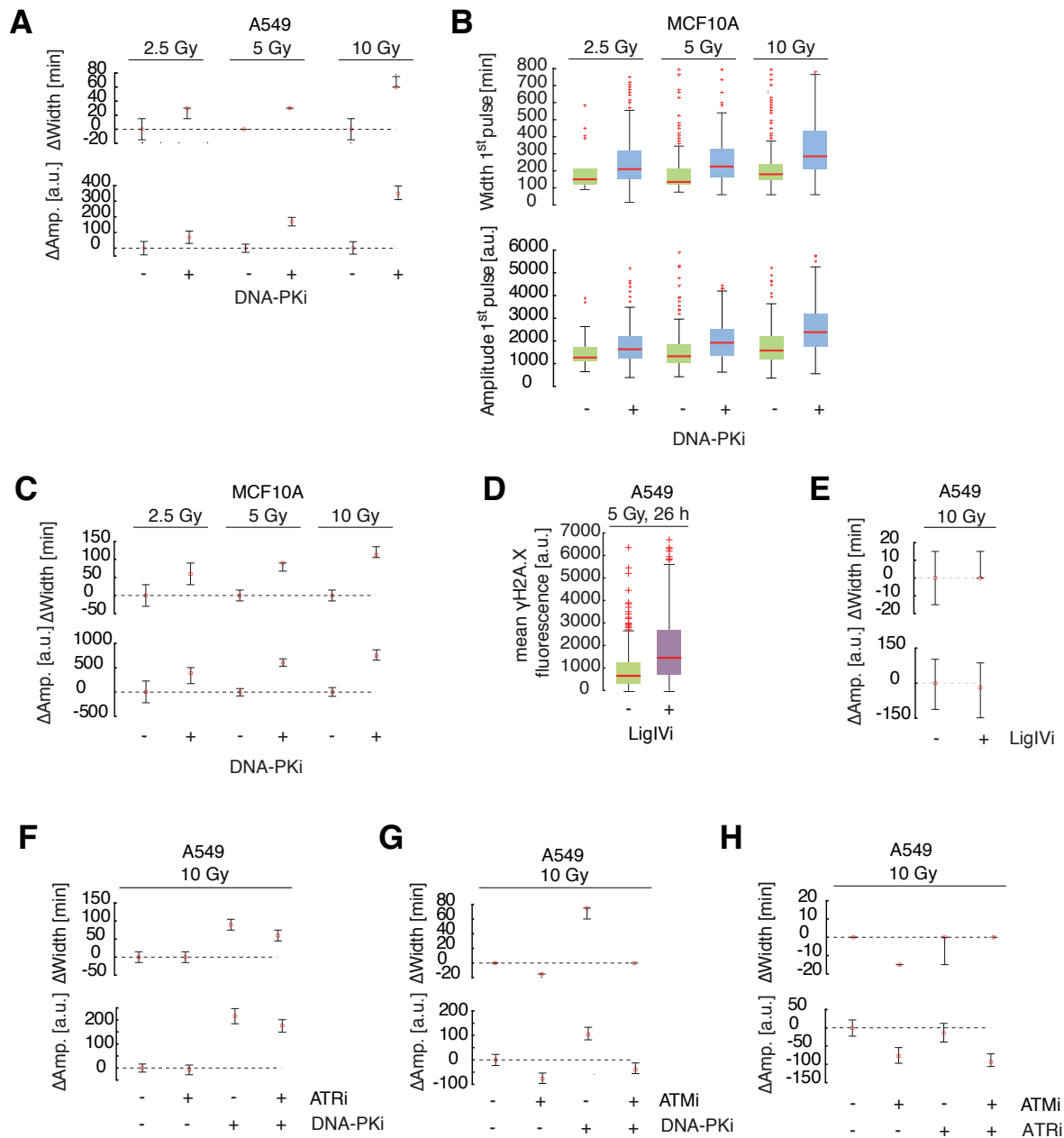


**Figure S3.** (A) Statistical analysis corresponding to Figure 2C. (B-C) Quantification of the relative amplitude and FWHM of the first p53 pulse upon 2.5, 5 or 10 Gy in cells untreated or treated with DNA-PKi in MCF10A cells and corresponding statistical analysis (error bars represent 90% confidence intervals,  $n > 28$  cells per condition). (D) Quantification at 26 hours of the  $\gamma$ H2A.X average nuclear fluorescence intensity upon 5 Gy  $\gamma$ -IR in A549 cells untreated or treated with LigIV inhibitor. ( $n > 340$  cells per condition). (E-H) Statistical analysis corresponding to Figure 2D (E); 3A (F); 3B (G); 3C (H). Estimated changes of the median pulse width and amplitude (red dots); error bars represent 90% confidence intervals.

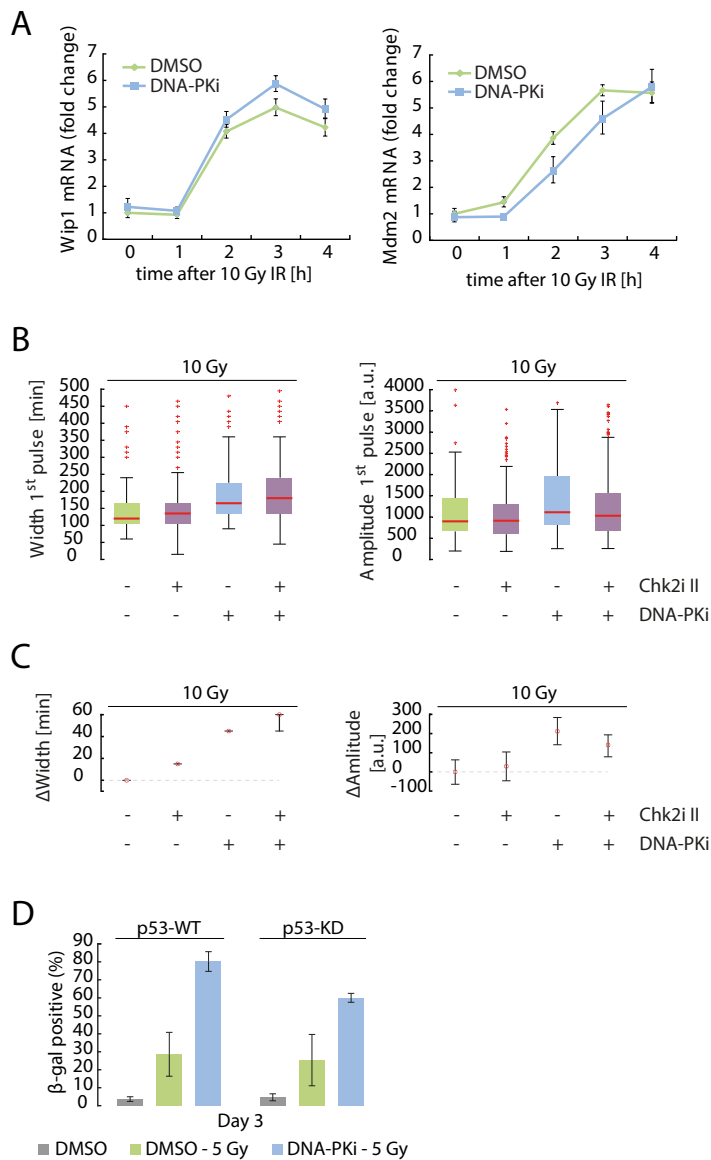


**Figure S4.** (A) mRNA expression of p53 negative feedback regulators Wip1 and Mdm2 was measured upon 10 Gy  $\gamma$ -IR in A549 cells untreated or treated with DNA-PKi.  $\beta$ -actin was used as an internal control. Error bars indicate standard deviation of technical triplicates. (B) Quantification of the relative amplitude and FWHM of the first p53 pulse upon 10 Gy  $\gamma$ -IR in A549 cells untreated or treated with DNA-PKi and Chk2i II alone or in combination. ( $n > 150$  cells per condition). (C) Statistical analysis corresponding to Figure S4B. Estimated changes of the median pulse width and amplitude (red dots); error bars represent 90% confidence intervals. (D) Percentage of  $\beta$ -galactosidase-positive A549 cells 3 days post damage (5 Gy  $\gamma$ -IR) in wild-type (wt) or p53 knockdown (kd) conditions both in the presence or absence of DNA-PKi. Error bars indicate the standard deviation of three independent experiments with more than 100 quantified cells per each condition.